ACS APPLIED MATERIALS & INTERFACES

RESEARCH ARTICLE

www.acsami.org

# Transparent, Luminescent, Antibacterial and Patternable Film Forming Composites of Graphene Oxide/Reduced Graphene Oxide

T. S. Sreeprasad, M. Shihabudheen Maliyekkal, K. Deepti, K. Chaudhari, P. Lourdu Xavier, and T. Pradeep*

DST Unit of Nanoscience, Department of Chemistry, Indian Institute of Technology Madras, Chennai-600 036, India

Supporting Information

**ABSTRACT:** Multifunctional graphene oxide/reduced graphene oxide (GO/RGO) composites were prepared through electrostatic interaction using biocompatible ingredients. Different functionalities were added to GO/RGO by anchoring materials such as native lactoferrin (NLf), NLf protected Au clusters (designated as Au@NLf), chitosan (Ch) and combinations thereof. Anchoring of Ch and NLf enhances the antibacterial property of RGO/GO. The addition of Ch to RGO/GO not only helped in forming stable dispersions but also helped in fabricating large ($cm^2$) area films through a simple solvent evaporation technique. Functionalities such as photoluminescence were added to Ch-RGO/GO composites by anchoring Au@NLf on it. The composites thus formed showed stable luminescence in presence of various metal ions in the solid state. The composite showed reasonable stability against pH and temperature variations as well. The as-prepared films were transparent and the transparency could be modulated by controlling the concentration of RGO/GO in the composite. The antibacterial property and ability to form stable thin films may provide an opportunity to use such composites for medical and environmental remediation applications as well. Erasable patterns were fabricated on the film by stamping required patterns under compressive pressure. Luminescent patterns can be inscribed on the film and can be erased by simply wetting it. Such films with erasable information may be useful for security applications.

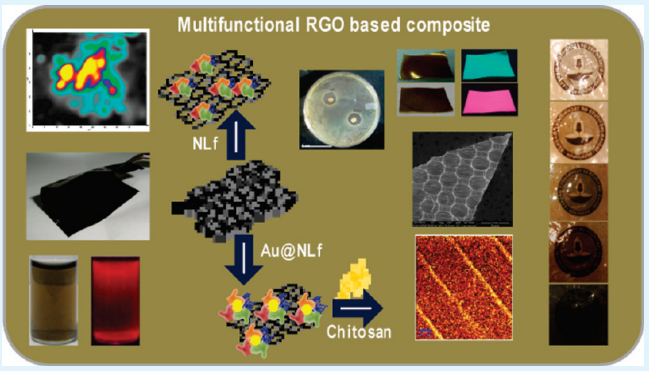


**KEYWORDS:** reduced graphene oxide, quantum clusters, luminescent films, composites, chitosan, antibacterial

## INTRODUCTION

Graphene[1] an exciting carbon based material, owing to its perfect 2D structure and associated properties has been envisaged to be a promising material for many futuristic applications.[2−6] The high mechanical stiffness[7] and excellent electron transport properties[8,9] makes it a highly attractive research material. Special properties of graphene, such as remarkable thermal conductivity,[10] ambipolar field effect,[1] room temperature quantum Hall effect,[8] tunable band gap,[11] and high elasticity[7] have all been documented in the literature. Reaping the benefits of these properties require bulk synthesis of graphene. Conventional method of physical exfoliation of graphite to graphene has the inherent limitation of poor yield.[1] Chemical methods offer an alternate way for this. Many routes like chemical vapor deposition,[12] chemical reduction of graphite oxide (GO),[13] nanomaterial based reduction,[14] liquid-phase exfoliation of graphite,[15] and the self-assembly approach,[16] have been tried so far for the bulk production of graphene. However, the reduction of GO to reduced graphene oxide (RGO) under chemical or hydrothermal conditions seems to be simple and comparatively successful in large-scale synthesis.

Graphene composites generally have superior properties and utility. Various application possibilities of graphene and their composites in transistors,[17,18] solar cells,[19,20] and sensors[21] have been demonstrated. Very recently, they have found place in water purification,[22,23] and biological[24−27] applications as well. Graphene based biocompatible paper was prepared and its biocompatibility was demonstrated by culturing mouse fibroblast cell line (L-929).[27] The cell lines were found to adhere to and proliferate on graphene papers. A subconfluent layer of metabolically active cells were formed within 48 h of culture time. Agarwal et al. tested biocompatibility of RGO with rat pheochromocytoma (neuroendocrine cell, PC12) cells, human oligodendroglia (HOG) cells and human fetal osteoblast (hFOB) cells[26] and found that RGO is biocompatible with all the cells tested. PEGylated GO/RGO were also used for cellular imaging and drug delivery applications.[25] Very recently, Hu et al. found that graphene, though is compatible with human cells, has antibacterial property.[24] Recent investigations shows that RGO/GO and their composites are good adsorbent media for the removal of heavy metals from water. RGO-magnetite and GO-ferric hydroxide composites were used for the removal of arsenic from water.[23] Sreeprasad et al. showed that the Hg(II) uptake capacity of RGO can be enhanced by decorating RGO

Received: April 11, 2011
Accepted: June 20, 2011
Published: June 20, 2011

  

sheet with silver or manganese oxide nanoparticles.[22] Their studies clearly demonstrated the superiority of RGO/GO composites over parent RGO/GO due to synergetic effect from the combination of materials.

Atomically precise clusters of noble metals are a new family of materials with intense luminescence and other properties.[28,29] Among them, protein stabilized clusters[30,31] are attracting attention these days in view of their utility in biological imaging.[30,31] Lactoferrin (Lf) is a multifunctional glycoprotein of transferrin family with two ferric ion binding sites per protein which in native (N) state is called NLf.[32] Au clusters made within NLf exhibit strong luminescence centered at 660 nm, when excited at 380 nm.[30] Here, we prepared multifunctional GO/RGO-based composites with NLf and Au@NLf. The composite formation was assisted by chitosan (Ch), a biopolymer. These ingredients were selected for combining various attributes such as antibacterial property, luminescence, and free-standing film formation. Luminescence functionality was added to the composite by anchoring Au@NLf clusters on RGO/GO. Large area (of the order of $cm^2$ area) films were fabricated from the composites. The bactericidal ability of the composite was examined. Luminescent RGO/GO based films were also made and it was found that the luminescence is stable under various environmental conditions and against various metal ions. The antibacterial films thus made may be useful in water purification and medical applications. For example, as an antibacterial coating agent on membranes (e.g., reverse osmosis membrane) and medical devices (e.g., catheter), which are highly susceptible to contamination due to microbial growth. Luminescent patterns can be inscribed on the film and can be erased by simply wetting the film. In short, new RGO/GO based composites were prepared and their possible utility in various applications were demonstrated.

## EXPERIMENTAL METHODS

**Materials.** Natural graphite was purchased from Active Carbon India Pvt. Ltd., India. Sulfuric acid ($H_2SO_4$, 95−98%), hydrochloric acid (HCl, 36%) and $CuCl_2.2H_2O$ were purchased from Ranbaxy Chemicals, India. Phosphorus pentoxide ($P_2O_5$), hydrazine monohydrate ($N_2H_4 \cdot H_2O$, 99−100%), hydrogen peroxide ($H_2O_2$), were purchased from SD Fine Chemicals, India. Potassium peroxydisulfate ($K_2S_2O_8$) was purchased from Sisco Research Laboratories Pvt. Ltd., India. Potassium permanganate ($KMnO_4$) was purchased from Merck. Tetrachloroauric acid trihydrate ($HAuCl_4.3H_2O$) was purchased from CDH, India. Chitosan was procured from Pelican Biotech & Chemical Laboratories, India. Native bovine lactoferrin (NLf, ∼17.5% iron saturated, purity >96%) of Taradon Laboratory was supplied by the company, Tablets India Pvt Ltd., Chennai, India. The purity of the protein was tested by sodium dodecyl sulfate polyacrylamide gel electrophoresis (SDS−PAGE) and matrix assisted laser desorption ionization time-of-flight mass spectrometry (MALDI−TOF MS) and no impurities were detected. All chemicals were used as received without any additional purification. Triply distilled water was used all through this study.

GO synthesis from graphite powder was carried out based on the modified Hummers method reported by Kovtyukhova et al.[33] It involves two steps: (a) preoxidation of graphite and (b) oxidation of preoxidized graphite. Detailed procedure is given in Supporting Information S1. The reduction of GO to RGO was done hydrothermally following a reported procedure.[34] To increase the stability of RGO in water, sulfonic acid groups were introduced onto RGO surface through a simple sulfonation procedure (Supporting Information S1).[35] Using GO and RGO, composites were fabricated. Similar experiments were done using chemically reduced GO as well.[13]

**Preparation of Au@NLf.** Au@NLf quantum clusters were synthesized according to a procedure reported by our group.[30] Briefly, NLf and $HAuCl_4$ were mixed and stirred continuously for 5 min. Required amount of 1 M NaOH was added to the above mixture such that the final concentration was 5%. The mixture was stirred for 24 h which results in the formation of Au@NLf. Detailed procedure is given in Supporting Information S1. Au@NLf refers to a mixture of clusters, dominated by a cluster containing 25 atoms of gold, along with minor fractions of $Au_{13}$, which are protected by the protein molecule (see below).

**Preparation of RGO/GO-NLf and RGO/GO-Au@NLf composites.** NLf was anchored onto RGO/GO substrate through a simple electrostatic interaction. To 5 mL GO/RGO (0.02 wt %), different volumes of NLf (12 mg/mL) was added. The sample was stirred for 2 h and stored at 4 °C for further use. Similar strategy was adopted to make GO/RGO-Au@NLf composites in which known volume of Au@NLf was added to 5 mL of GO/RGO and stirred for 2 h. The mixture was stored for further use at 4 °C.

**Preparation of RGO-NLf-Ch Composite.** Ch is known to form composites with RGO.[36] GO/RGO-NLf composites prepared as mentioned above were mixed with Ch solution (0.8% chitosan in 1.5% acetic acid) in 1:0.3 ratio (v/v). The mixture was stirred continuously for 2 h. After 2 h, the homogeneous dispersion was kept at 4 °C for further use. Similarly, GO/RGO-Au@NLf-Ch was also prepared by replacing NLf with Au@NLf in the above procedure.

**Preparation of RGO-Ch-NLf/Au@NLf Film.** The above solution was transferred to a Petri dish and kept in an oven maintained at 40 °C. The mixture was allowed to dry and after complete drying, the film was immersed in ammonia solution (5 vol %) for 15 min. Then, the films were washed repeatedly with distilled water to remove ammonia. This film can be easily peeled off for further use. For preparing red luminescent films, NLf was replaced with Au@NLf clusters. RGO-Ch composites without NLf were also fabricated.

**Kerley-Born Diffusion Test.** In order to qualitatively evaluate the antibacterial ability of the composite, a Kerley-Born diffusion test was carried out. A bacterial (E-coli) test dilution was seeded into Petri dish with EMB agar and spread all over the agars with the help of L-shaped glass rod. Then 2 disks impregnated with a 300 $\mu$L of RGO-Ch-NLf and GO-Ch-NLf were placed on the agar medium. The impregnated sample diffuses around the paper disk, forming a radial decreasing concentration gradient of the sample. The Petri dishes were incubated for 16 h at 37 °C and the ability of the sample to inhibit the growth of the organism is indicated by a zone of inhibition around the disk.

**Optical Density Test.** A direct turbidity measurement using spectrophotometer was also carried out to check the cell viability in presence of the samples. For this, 10 mL of sterile agar medium were taken in 50 mL sterile test tubes. Known quantities of the samples were then added to the test tubes and dispersed homogeneously. The reactors were then seeded with freshly cultured bacterial cells (E-coli). The initial optical density (OD) at 600 nm of the sample was measured to be 1.85. The test tubes were then incubated for 16 h at 37 °C and the OD at 600 nm were recorded. All measurements were done in triplicate and average value is reported.

**Instrumentation.** UV/vis spectrum of each sample was measured using a Perkin-Elmer Lambda 25 UV/vis spectrophotometer. ATR IR measurements were done using a PerkinElmer, Spectrum 100 spectrometer. The samples were freeze-died and spectra were measured. Samples were examined using a JEOL 3011, 300 kV high resolution transmission electron microscope (HRTEM) with a UHR polepiece. Samples were dropped onto a carbon-coated copper grid at specific reaction time and dried in the ambient conditions for measurements. Raman spectra were measured with a WiTec GmbH confocal micro

**Scheme 1. Various Composites Made and Their Proposed Utility**

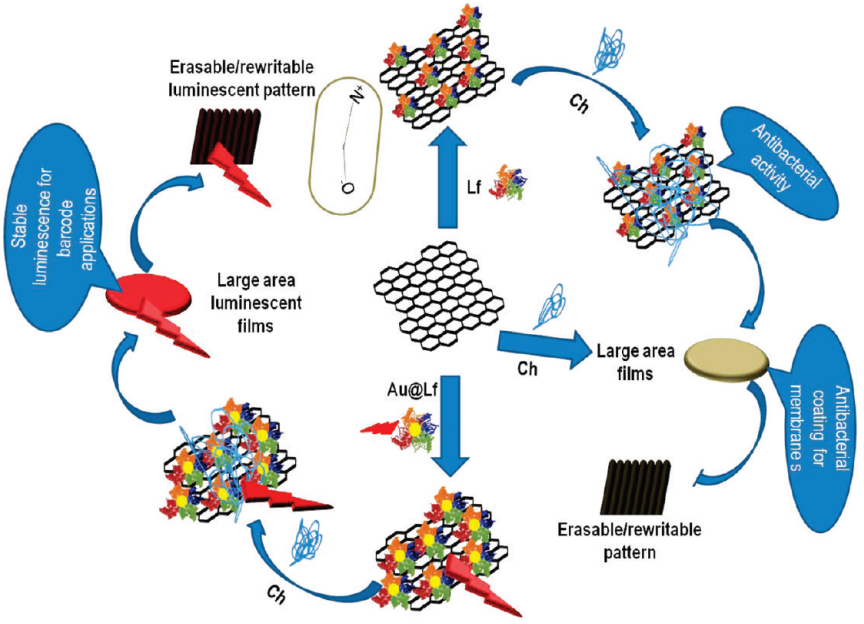


Raman spectrometer. XPS measurements were done with Omicron ESCAProbe spectrometer with unmonochromatized Mg Kα X-rays ($h\nu$ = 1253.6 eV). Six spectra in the desired binding energy range were averaged. The samples were spotted as drop cast films on the sample stub and dried. The energy resolution of the spectrometer was set at 0.1 eV at a pass energy of 20 eV for typical measurements. Matrix-assisted laser desorption ionization mass spectrometry (MALDI-MS) studies were conducted using a Voyager-DE PRO Biospectrometry Workstation from Applied Biosystems. A pulsed nitrogen laser of 337 nm was used for the MALDI-MS studies. Mass spectra were collected in the positive-ion mode and were averaged for 100 shots. Fluorescence spectra were measured with a Nanolog HORIBA JOBI-NYVON spectrofluorimeter with a 100 W xenon lamp as the excitation source at a scan speed of 240 nm/s. The band-pass for both excitation and emission monochromators was kept at 5 nm. SEM images were taken with FEI quanta 200.

A schematic summary of the different stages of composite formation and methodology used is depicted in Scheme 1. Different proposed utilities are also given.

## RESULT AND DISCUSSION

Protien protected clusters are interesting due to their wide range of application possibilities especially in biological systems. Au@NLf clusters were prepared by a reported methodology[30] and were characterized. Sinapinic acid mixed with urea was used as the matrix for the MALDI measurements. The mass spectrum of NLf showed two distinct peaks at 41.5 and 83.0 kDa due to the di- and mono-cations (Supporting Information, Figure S2A). The cluster sample showed a major peak at $m/z$ 83,024 corresponding to NLf and two distinct, but low intensity peaks at $m/z$ 85,570 and 87,965 were also seen. From the mass spectrum, the cluster core was assigned as $Au_{25}$ (peak at $m/z$ 87,965) which is encapsulated in the protein. A small fraction seen at $m/z$ 85,570 was assigned as $Au_{13}$. The cluster and protein were characterized by fluorescence spectroscopy as well (Supporting Information, Figure S2B). For Au@NLf clusters, when excited at 380 nm, two peaks where observed. The first is one at 450 nm, corresponding to the weak luminescence of the protein (observed upon excitation of protein alone at 380 nm) and another is at 650 nm assigned to the cluster core. They were analyzed using UV/vis spectroscopy as well (Supporting Information, Figure S2C). Protein showed a strong feature around 280 nm due to the presence of aromatic amino acids in it. Au@NLf did not show any prominent feature. But a feature (dampened compared to the protein feature) at 280 nm was seen which was attributed to the protein covering. In TEM, these clusters were seen as subnanometer regime particulates (marked in Supporting Information, Figure S2D).

Water solubility of RGO was enhanced by sulfonation. The presence of sulfonic acid groups on RGO was confirmed by ATR-IR measurements (Supporting Information Figure S3) which showed characteristic peaks at 1125, 1035, and 1007 $cm^{-1}$.[35] GO is known to be highly dispersible in water and large area films were seen on the TEM grids (Supporting Information Figure S4). RGO after sulfonation was seen to be highly dispersible in water and large area films were seen (Supporting Information Figure S4). Sulfonation of RGO introduced additional negative functional groups in the form of sulfonic acid groups. Different functionalities were added to RGO through electrostatic interaction. Presence of carboxylic and sulfonic acid groups in the ionized form aided the composite formation. The functionalities added to RGO through the formation of composite include, photoluminescence, antibacterial property, and free-standing film formation which are discussed below.

**Addition of Luminescence.** Limited efforts have been made to incorporate luminescence to graphene.[37−39] Two main routes to incorporate luminescence to graphene are (i) by cutting graphene into ribbons and quantum dots and (ii) by chemical or physical treatments, to reduce the connectivity of the $\pi$-electron network.[37] Attachment of luminescent molecules to GO/RGO chemically is an alternative.[37−39] But this method has seen little progress since the direct bond formation between the fluorophore and RGO creates an alternate pathway for the decay of excited state energy, thereby quenching the luminescence.[37−39]

An alternate and more feasible way is to avoid direct covalent bond and to anchor the luminescent agent through noncovalent interactions such as electrostatic interaction. Here we anchored a luminescent iron binding protein, lactoferrin (NLf) or NLf protected Au clusters (Au@NLf) electrostaticlly at nearly neutral pH. The pH of GO and RGO dispersion was around 6.5. At this pH, the negatively charged functional groups will be in the ionized state making GO and RGO highly dispersible in water. The presence of negatively charged functional groups on RGO/GO was utilized for the formation of composites. The samples were characterized by Raman spectroscopy which showed a strong D-band pointing to the highly functionalized graphene (Supporting Information Figure S4).

Lf, a glycoprotein is reported to have antimicrobial, antiviral, immunomodulation, antioxidation, anti-inflammation, antistress, and analgesic properties.[32] NLf has a p$K_a$ of ~8.5 and will have a positive charge at the pH of RGO/GO (~6.5). Thus the addition of NLf into RGO/GO results in the formation of a composite with strong electrostatic interaction between the negative functional groups on GO (carboxylic, hydroxyl, etc.)/RGO (carboxylic and sulfonic acids) and positive (—$NH_3^+$ or ═$NH_2^+$) groups on the protein. The composite exhibited a weak bluish-green luminescence. Bright red luminescence was imparted to the composite by anchoring the protein protected clusters (Au@NLf) instead of pure NLf.

Figure 1 shows the characterization of GO/RGO-NLf composite. Figure 1A shows the UV/vis spectrum of GO-NLf composite. GO to begin with has a feature at 230 nm.[14] NLf had an absorption maximum at 280 nm due to the absorption of aromatic amino acids present in the protein.[30] As NLf was added to GO, the absorption due to GO was not visible and the absorption maximum at 280 nm, due to protein, became progressively visible. Similar observation was seen in the case of RGO as well (Figure 1B). The peak at 270 nm due to RGO dampened and a new peak at 280 nm emerged because of the presence of protein. When Au@NLf was added to GO/RGO similar changes in spectral features were observed (Supporting Information Figure S6). This is understandable since NLf is reported to retain its identity in Au@NLf as well, and no additional features were present for Au@NLf.[30] Composites were analyzed using ATR-IR to confirm their formation. Samples were freeze-dried and IR spectra were measured (Figure 1C). The characteristic stretching and bending vibrations of proteins due to amide bonds which link amino acids such as amide I (1634 $cm^{-1}$), amide II (1538 $cm^{-1}$), amide III (1241 $cm^{-1}$) and amide A (3300 $cm^{-1}$) can be seen in the composite, confirming the presence of NLf.[40] Bands at 2960 $cm^{-1}$ can be attributed to C—H vibrations.[40] The features around 1375 $cm^{-1}$, 1125 $cm^{-1}$, and 1040 $cm^{-1}$ indicate the sulfonated RGO in the composite.[35] Broad feature seen around 3500 $cm^{-1}$ is ascribed to OH stretching vibrations.[14,35] The presence of features due to NLf and RGO points to the composite formation.

The composites were characterized using transmission electron microscopy (TEM) as well. Figure 1D shows the large area TEM image of RGO-Au@NLf composite. We can see a large sheet of RGO onto which clusters are anchored. HRTEM analysis of initial GO or RGO showed large thin transparent sheets spread over $\mu m^2$ of area with characteristic wrinkles (Supporting Information Figure S5). After formation of composites also, the presence of wrinkles on the sheets confirmed the graphenic nature of the composite. Au quantum clusters are not seen in the large area image due to their smaller size. But upon

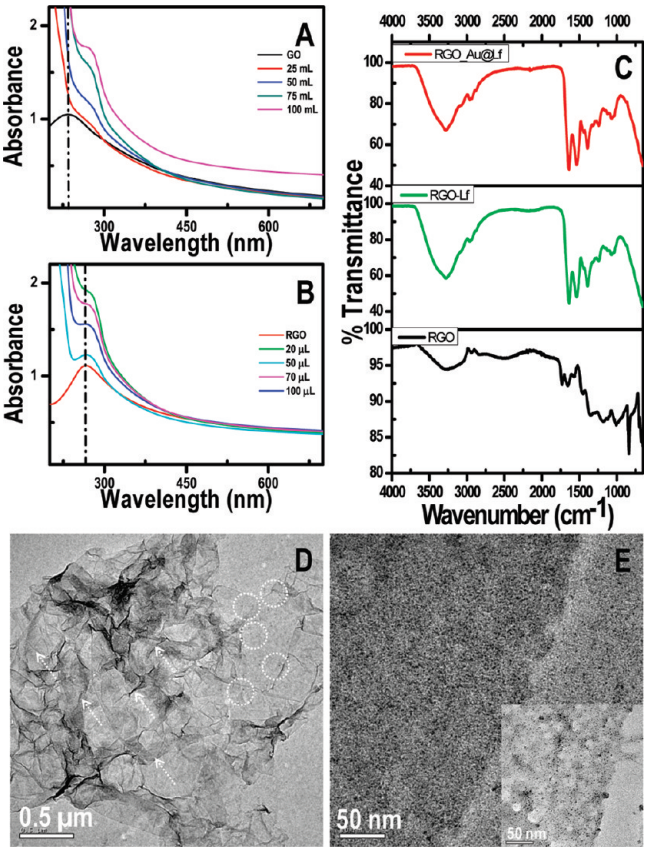


**Figure 1.** UV/vis spectra of (A) GO-NLf and (B) RGO-NLf composites. Spectral positions of GO and RGO are marked in the respective figures. (C) FTIR spectra of RGO-NLf and RGO-Au@NLf composites are compared along with that of RGO. (D) Large area TEM image of RGO-Au@NLf composite. Foldings of graphene sheets are marked by dotted arrows. Small dots seen on the sheets (marked by dotted circles) could be small aggregates of clusters. (E) Higher magnification image of an edge of an RGO sheet showing the anchored small clusters. Inset of E shows the same region after e-beam exposure for 20 min, showing bigger nanoparticles.

closer observation, some aggregates of the clusters (marked by dotted circles) can be seen in the figure. Figure 1E shows higher magnification image of one edge of the composite. We can see that the clusters are anchored onto the RGO sheets. Au quantum clusters are known to be sensitive toward e-beam irradiation.[41] Upon e-beam exposure, they aggregated to form bigger nanoparticles. Similar observation was seen in the case of RGO-Au@NLf composite as well. As the e-beam exposure time increased, the small clusters increased in size and ultimately formed nanoparticles (Supporting Information Figure S7). Inset of Figure 1E shows the same region after e-beam exposure. We can see large number of nanoparticles preferentially attached onto RGO sheets. Outside the RGO sheets, very few nanoparticles were present. This again confirms the composite formation, which preferentially attaches QCs onto the RGO surface.

The composite appears in the optical image (Figure 2A). It was analyzed by Raman spectroscopy (inset of Figure 2A). Spectrum shows essentially a luminescence background due to the presence of Au@NLf clusters. Note that Au@NLf is luminescent and shows an emission at 660 nm upon 380 nm excitation. As the laser source is 532 nm, an emission in this

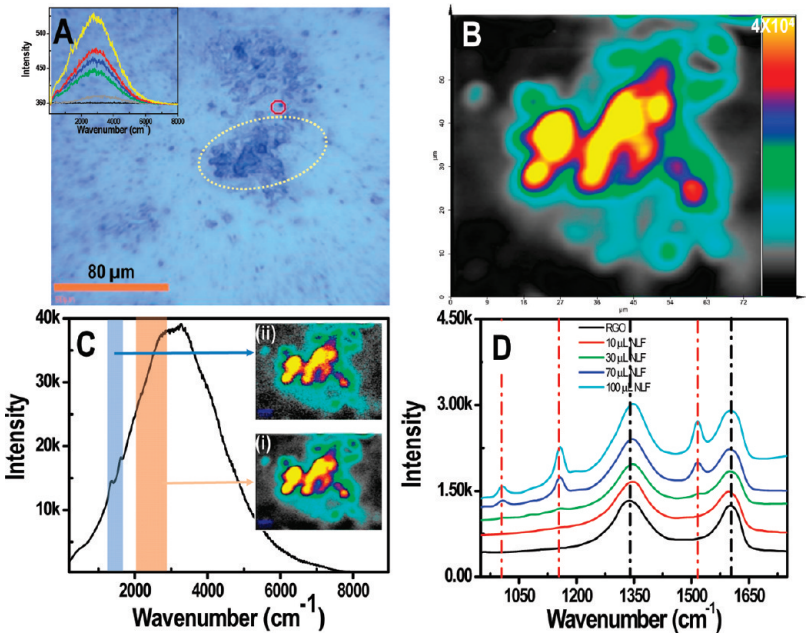


**Figure 2.** (A) Optical image of the composite under white light illumination. (B) Raman image taken from the composite, from the region marked by white circle in A. Inset in A is reconstructed image spectra from different parts of B. Colors of the spectrum corresponds to the regions in the image from where the spectrum is generated. (C) Single Raman spectrum taken from the composite showing the characteristic fluorescence from Au@NLf and D- and G-bands of RGO. Insets show the Raman spectral image generated from the Raman frequency range of 1700−2600 $cm^{-1}$ (i) Image corresponding to fluorescence from Au@NLf and from the Raman frequency range of 1300−1600 $cm^{-1}$ and (ii) corresponding to D-and G-bands of RGO confirming its presence. The 1:1 correspondence between (i) and (ii) supports the formation of the composite. (D) Raman spectra in the range of 950−1750 $cm^{-1}$, collected from RGO-NLf composite having different NLf content. The spectral features of RGO are marked with black lines and those of protein are marked with red lines.

window (corresponding to 3000 $cm^{-1}$ in Raman shift) is expected. Besides this, the spectrum shows the D and G bands of RGO at 1336 $cm^{-1}$ and 1587 $cm^{-1}$ respectively. Figure 2B shows the Raman image collected from the region marked by dotted circles in the optical image (Figure 2A). The reconstructed image spectra collected from different regions of the composite (RGO-Au@NLf) are given in the inset of Figure 2A. Colors of the spectra presented in the inset of Figure 2A correspond to the colors of the region in the Raman image from where the spectra are generated. In all the spectra, G- and D-band due to RGO and the luminescence background due to the anchored clusters can be seen, pointing to the formation of a nanocomposite. A large characteristic fluorescence background peaking around 3000 $cm^{-1}$ confirms the presence of Au@NLf cluster and the D and G bands confirms the presence of RGO. Hence, the composite formation was clear from the Raman spectrum. Inset image (i) in Figure 2C shows the Raman spectral images generated from the Raman frequency range of 1700−2600 $cm^{-1}$ (where GO/RGO does not have any feature), corresponding to luminescence from Au@NLf, showing presence of the cluster. Raman spectral image generated from the frequency range of 1300−1600 $cm^{-1}$ (corresponding to D-and G- bands of GO/RGO) confirms the presence of RGO (Inset image ii). We can see a 1:1 correspondence between images, pointing to the formation of RGO-Au@NLf composite. Raman spectrum of the composite in the lower wavenumber region is expected to show Raman features due to NLf. However, in the case of RGO/GO-Au@NLf composite, the huge fluorescence background masked the features of NLf. But in the case of RGO−NLf (Figure 2D), NLf features were seen. Figure 2D shows the spectra collected from RGO-NLf composite with varying NLf content. As the NLf content in the composite increases, peaks due to NLf (marked by red lines) became more and more prominent. Graphenic features, G- and D-band (marked by black line) did not show any shift, indicating that the chemical nature of RGO remains same after the formation of composite. The spectra in this case were collected with 633 nm to reduce the luminescence background.

To improve the properties of the above composites, chitosan (Ch), a naturally occurring biopolymer was incorporated into the composite. Ch is a biocompatible[42−45] polysaccharide composed of $\beta$-(1−4)-linked D-glucosamine (deacetylated unit) and *N*-acetyl-D-glucosamine (acetylated unit). It has been used for various applications including drug delivery,[43,44] for fabricating implantable scaffolds, etc.[45] Bacteriostatic property of Ch which enhances healing rates of wounds is well-known.[43] The ability of Ch to enhance the strength and dispersibility of RGO is documented.[36,46] The presence of Ch in the composite was confirmed using IR spectroscopy (Supporting Information Figure S8). The luminescence of the prepared composites was analyzed using fluorescence spectroscopy (Figure 3). Photoluminescence spectra of the ingredients used for fabricating the composite are given in the Supporting Information (Supporting Information Figure S9). All the constituents in the composite have an excitation wavelength of 370 nm and hence can be excited simultaneously to give a combined desired emission. Figure 3A−D shows the photoluminescence spectra of various GO based composites. Figure 3A shows the photoluminescence of GO-NLf composite. The corresponding photographs in the visible and UV lights are also given in the respective figures. Excitation at 370 nm yielded an emission around ~450 nm. The emission at 450 nm is attributed to the tryptophan residue of the

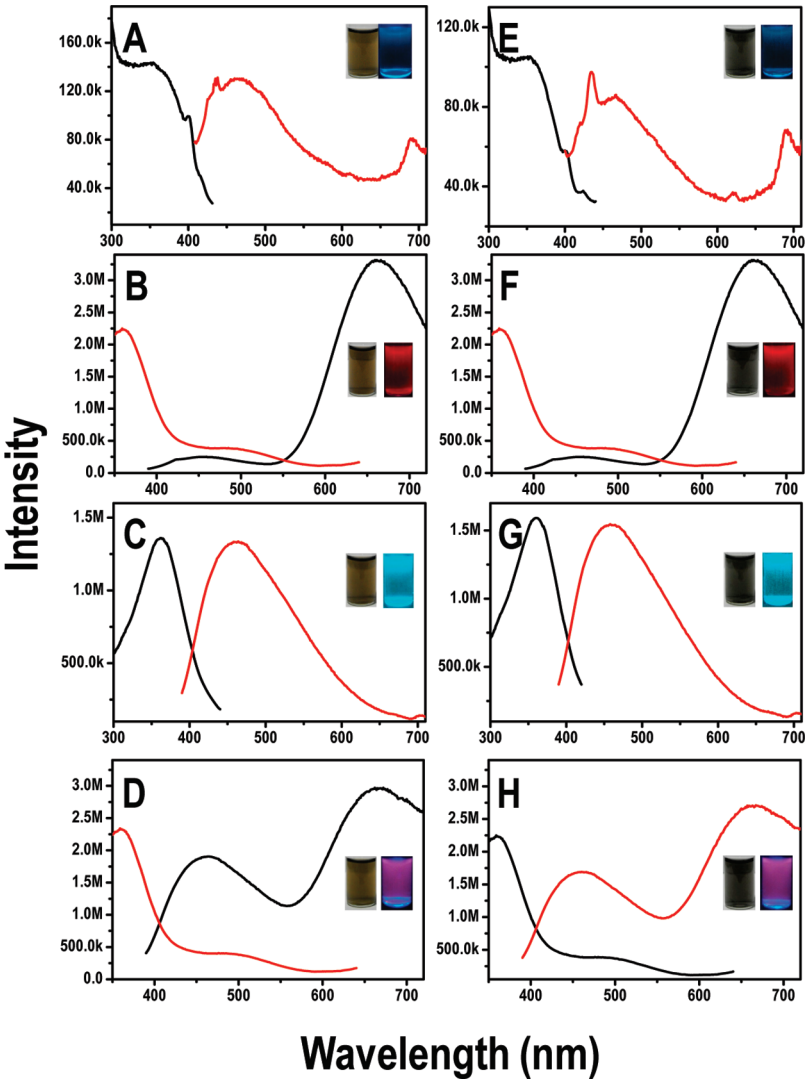


**Figure 3.** Photoluminescence spectra of different composites (A) GO-NLf, (B) GO-Au@NLf, (C) GO-Ch-NLf, (D) GO-Ch-Au@NLf, (E) RGO-NLf, (F) RGO-Au@NLf, (G) RGO-Ch-NLf, and (H) RGO-Ch-Au@NLf. Insets of each figure are the photographs of the samples under visible (left) and UV (right) light showing the visible luminescence.

protein.[30] But, the intensity is comparatively low. However, in the case of GO-Au@NLf clusters, excitation at 370 nm gave a prominent emission around 660 nm. A weak emission was seen around 450 nm which confirms the presence of the protein.[30] The spectrum showed close resemblance with that of Au@NLf clusters.

Fluorescence resonance energy transfer from tryptophan residues of NLf to the cluster is reported to be the reason for the emission at ~660 nm, when the protein is excited at 370 nm.[30] The similarity of the spectrum confirms that the characteristics of the cluster are retained in the composite. In the case of GO-NLf-Ch, a stronger emission was seen around ~450 nm. This may be due to the presence of Ch in the composite, which is known to have an emission at 450 nm (Supporting Information Figure S9). The composites appeared bluish-green under UV light. A similar observation was seen in the case of GO-Au@NLf-Ch composites as well. Emission peak around 450 nm increased in intensity due to the presence of Ch and the emission at 660 nm was very prominent emphasizing that the cluster core remains the same in the GO-Au@NLf-Ch composite. But, in the case of GO-Au@NLf-Ch, a visible color change from red to pink was observed under UV illumination. This was attributed to the presence of Ch in the composite which imparts a green tinge resulting in a combined effect of pinkish appearance under UV light. However, no appreciable shift was seen even after the formation of the composites in the photoluminescence spectrum. RGO composites showed similar spectral features as that of the corresponding GO composites (Figure 3E−H).

XPS measurements also supported the composite formation. Figure 4 shows the detailed XPS spectra of C 1s, S 2p, and N 1s for the various RGO-composites. Pure RGO showed two components in the C 1s spectrum. Prominent component ($C_1$) centered at 284.5 eV is attributed to nonoxygenated ring carbon. Additional component centered around 288.8 ($C_2$, C═O) was also observed.[47,48] Sulfur 2p, showed a peak centered at 169.6 eV, emphasizing the sulfonic acid groups present on the RGO.[49] Nitrogen 1s (Figure 4$C_1$) region did not show any feature, indicating the absence of N in the material. After the formation of RGO-NLf composite (Figure 4$A_2$−$C_2$), XPS

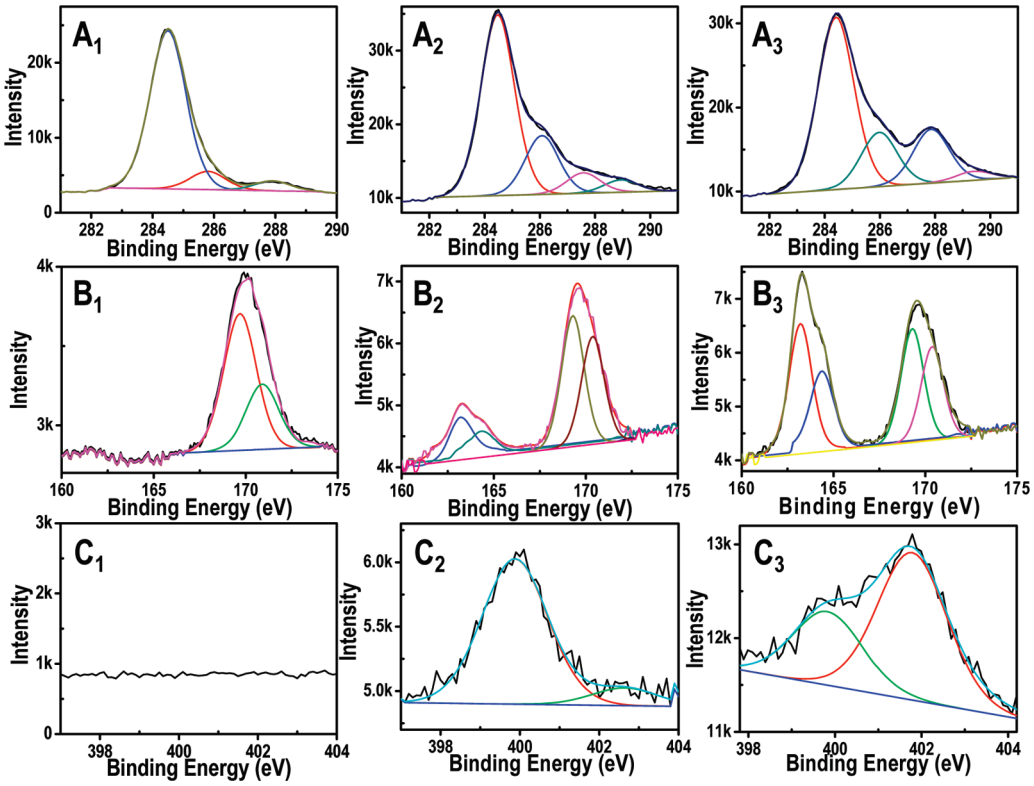


**Figure 4.** XPS spectra for RGO (1), RGO-NLf (2), and RGO-Ch-NLf (3) composites in the C 1s ($A_1-A_3$), S 2p ($B_1-B_3$) and N 1s ($C_1-C_3$) regions, of all the samples. Multiple features are fitted.

measurements showed interesting changes. In the C1s spectrum, four major components were seen, that is, $C_1$ (284.6) due to the nonoxygenated ring carbon from RGO, $C_2$ (286.3 eV) due to the C—N bond presumably from the presence of protein,[50] $C_3$ (287.6) due to C—O and $C_4$ (288.9) due to C═O.[47,48] Component $C_2$ establishes the presence of protein in the composite. S 2p showed two prominent features at 162 and 169 eV, due to thiols[51] (from the protein) and sulfonic acids (from RGO), respectively. Protein may undergo X-ray induced oxidation and hence the peak at 169 eV can have contribution from oxidized thiols as well.[47] N 1s spectra also confirmed the composite formation. N 1s had two components at 400.5 eV ($N_1$, amide), and 402.3 eV ($N_3$, protonated amine).[52] The prominent component is $N_1$, indicating the presence of protein in the sample. Since slightly acidic pH was maintained, all the amines were found to be protonated, which helps in anchoring proteins onto RGO electrostatically. No peak was observed at 398 eV, showing the absence of neutral amines in the sample.[52] For the chitosan containing sample (Figure 4$C_3$), N 1s spectra showed two components. However, the prominent component in this case was found to be $N_2$ pointing to the larger percentage of protonated amine entities.[52] Component $N_1$ was centered at 400.1 eV indicating the protein and thus confirming the formation of RGO-NLf-Ch composite. In the case of RGO-Au@NLf-Ch composite, prominent features of Au 4f and S 2p were seen emphasizing the presence of the cluster in the composite (Au 4f region is shown in Supporting Information Figure S10). The Au $4f_{7/2}$ appears at 84.0 eV supporting the fact that the metal is in zerovalent state due to the intact cluster.

**Antibacterial Studies.** Antibacterial agents such as quaternary ammonium compounds,[53] antibiotics[54] and metal ions[55] have been known for some time. All these materials have associated problems like the need of complex post treatment processes, environmental pollution, leaching and consequent short effective lifetimes, bacterial resistance, etc. Though nanomaterials like Ag nanoparticles,[56] $TiO_2$ nanoparticles[57], or carbon nanotubes[58] show enhanced antibacterial activity, they are known to show cytotoxicity as well.[58,59] RGO/GO may be a better alternative as they have much lesser cytotoxicity compared to other common antibacterial agents. The antibacterial activity of the various composites prepared was tested. Materials were added to different bacterial cultures having the same bacterial content and incubated for 24 h. A preliminary qualitative test (Kerley-Born diffusion test) was done to check whether the prepared material is antibacterial or not. Both the composites showed excellent antibacterial activity as can be seen from the zone of inhibition exhibited (Supporting Information, Figure S11).

In order to compare the antibacterial ability of the composite and its constituents, optical density test was conducted. Figure 5 shows the comparison of antibacterial activity of different materials studied. All materials selected showed antibacterial activity. But the composites; RGO/GO-NLf-Ch and RGO/GO-Au@NLf-Ch showed maximum activity due to the synergetic effect of the combination of materials. The antibacterial activity of the composites was found to be several folds higher than the parent GO/RGO. As all the ingredients used in the composite were biocompatible; the composites may find application as antibacterial agents.

**Large Area Film Fabrication.** Large area RGO/GO based composite films were fabricated through a simple self-drying methodology. Upon solvent evaporation, the composites formed

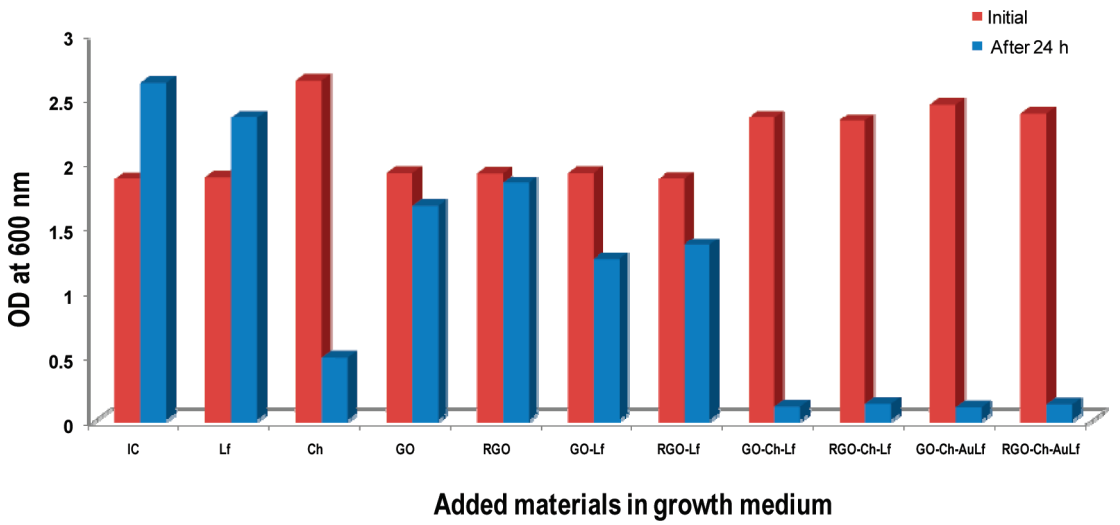


**Figure 5.** A comparison of antibacterial activity of different materials tested.

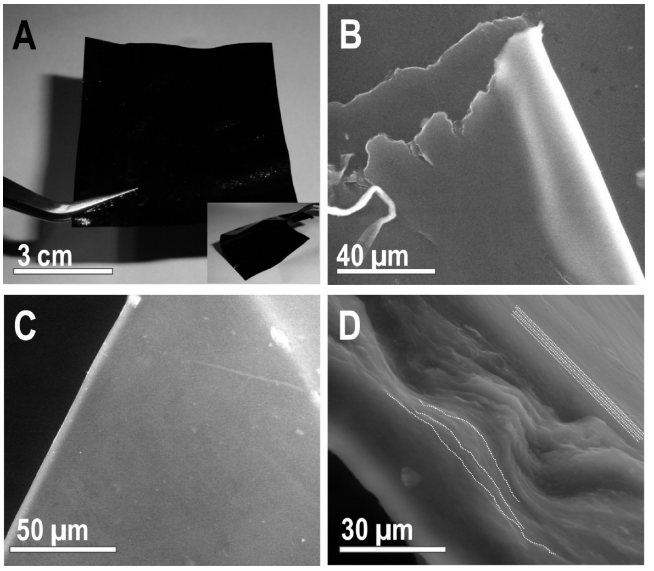


**Figure 6.** (A) Photograph of a large area composite film. Inset shows the photograph of the folded film showing the flexibility of the film. SEM images of the films showing (B) the folded film edge, (C) surface of the film, and (D) higher magnification image of a cross-section of the film showing the layer-by-layer nature of film formation. Multiple layers are visible.

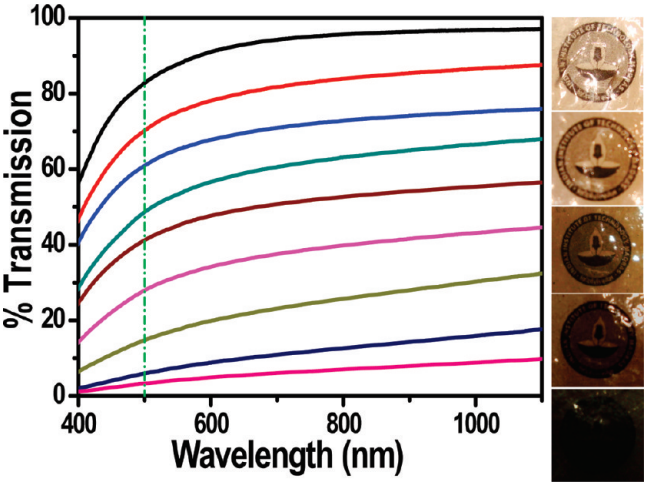


**Figure 7.** Transmittance curves of composite films having different RGO content showing the tenability of transmittance in the 400−1100 nm region. Corresponding representative photographs are also given.

large area films aided by Ch. The presence of RGO increased the mechanical strength of the film. Figure 6A shows the photograph of macroscopic films. The as-fabricated films were found to be highly flexible (inset Figure 6A). Film was characterized using SEM, Raman and fluorescence spectroscopy. Figure 6B−D shows the SEM images of the film. The SEM image of a folded edge of a film is shown in Figure 6B, emphasizing the flexible nature. The film surface was found to be smooth (Figure 6C). Higher magnification image of the edge of the film showed that it is formed by layer-by-layer assembly (Figure 6D).

Excellent optical transparency to visible and near-infrared light (380−1300 nm)[1,6] as well as excellent mechanical properties[7] of RGO suggest its utility in making transparent conductive films (TCFs). TCFs have wide range of applications as flat displays, optical communication devices, and solar cells.[60] Several approaches have been made to make large area RGO based transparent films.[60] All these methods have limitations such as high temperature for graphene growth, limited control over the film structures, need of sophisticated processing conditions, and the difficulty in transferring the films onto various substrates postsynthetically. Chemical methods were employed as an alternative.[61] These methods involve several tedious steps and various parameters have to be precisely controlled. Comparatively, the presented method of film formation is simpler. We found that the transmittance of the film can be modulated. Chitosan has a strong absorption centered around 300 nm with an onset from 500 nm.[62] RGO has an absorption around 270 nm with a constant background absorption due to the extended double bonded structure.[13] Hence, we found that the transmittance of the prepared films in the range of 500−1100 nm can be adjusted by varying the concentration of RGO in the composite. Figure 7 shows the transmittance curves of films having varying

concentration of RGO. We can see that the transmittance in the 500−1100 nm range can be effectively controlled. Below 500 nm and up to 300 nm, where Ch has a strong absorption, transmittance can be adjusted up to a certain extent. This opens up numerous application possibilities. The conductivity of the films is expected to be enhanced by the presence of RGO.[46] Conductivity of the fabricated film can be enhanced further by incorporating materials such as conducting polymers,[63] which enables applications as TCF in various areas.

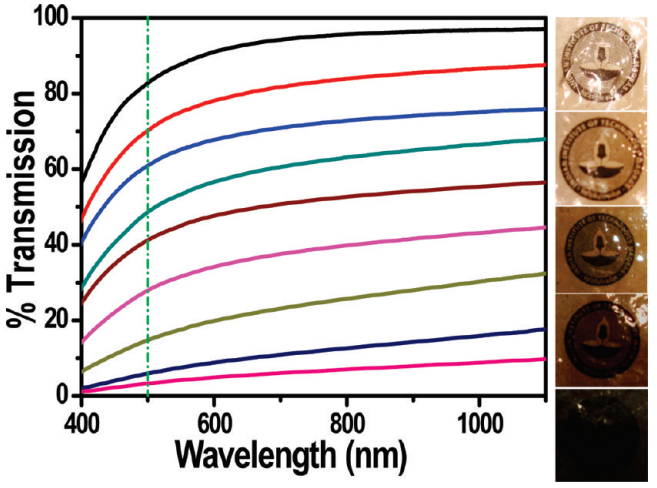


**Figure 8.** (A) Photographs of the composite films under visible and UV light; (B) corresponding solid state luminescence spectrum of the composites films made up of RGO-NLf-Ch (blue trace) and RGO-Au @NLf−Ch (red trace), and (C) plot depicting the stability of luminescence against various metal ions tested. Log of luminescence intensity of the film upon exposure to the metal ions is shown. Corresponding photographs of the film under UV light is also given. Higher order lines of the grating are shown by *s in B.

As discussed earlier, the luminescence quenching property of RGO makes it difficult to fabricate large area luminescent RGO based films. According to the best of our knowledge, no examples exist in the literature until date. In our methodology, the composite formation is through electrostatic attachment and direct bonding between RGO and the luminescent functionality is avoided. Figure 8A shows the photographs of GO-NLf-Ch and GO-Au@NLf-Ch films under visible and UV light. We can see that the films are brightly luminescent in the solid state under UV light. As-prepared luminescent film was examined using fluorescence spectroscopy. Figure 8B shows the corresponding solid state luminescence spectrum of the composite structures. In the liquid state, the emission maximum was around 660 nm and in the solid state it was centered around 670 nm. The spectrum corresponding to RGO-NLf-Ch is also given. The spectra were bit noisy in the solid state.

Luminescence of protein protected quantum clusters is known to be affected by metal ions and other environmental conditions such as pH and temperature.[28−31] This might be a limiting factor, when they are considered for sensing applications. Luminescence of these clusters is reported to be highly affected by ions such as $Cu^{2+}$.[28−31] After the formation of the composite, in the solid state, luminescence was found to be stable against a variety of metal ions tested, including $Cu^{2+}$. Figure 8C shows the stability of luminescence of the film against various metal ions. Corresponding photographs of the film under UV light is also given. We can see that the luminescence intensity remains almost constant in presence of various metal ions tested. In the case of RGO based films, as the SEM revealed, the surface was smooth and devoid of any micro pores. Quenching of luminescence upon addition of $Cu^{2+}$, in the case of protein protected Au clusters, is

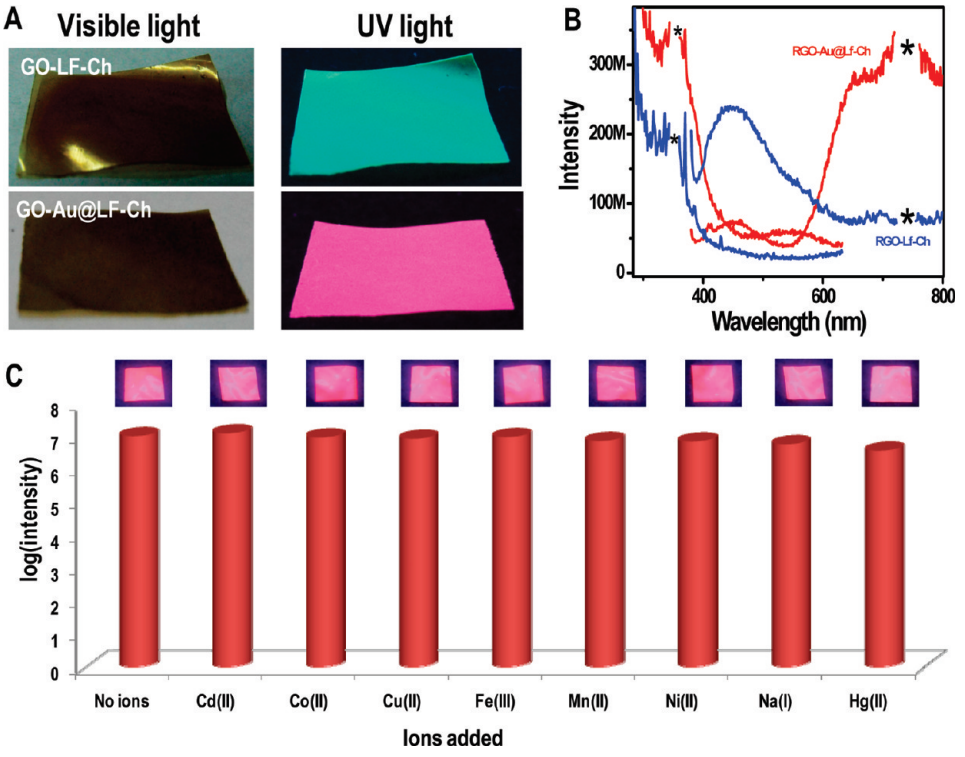


**Figure 9.** SEM images of different pattern ascribed on RGO composite films. A number of patterns are shown in A, C, and E and their expanded views are shown in B, D, and F, respectively.

reported to be due to the $Cu^{2+}$-induced aggregation of clusters.[31] In the composite, the clusters are anchored onto RGO/GO sheets. Hence, the freedom of movement for aggregation will be lesser. When Ch was added, it creates a stable matrix around the clusters which further restricts the freedom of motion and reduces the aggregation, thereby decreasing the tendency to quench the luminescence.

*5.2.1.3.1. Erasable Patterns and Security Application.* Large area patterns were inscribed on the prepared films. Patterns incorporating functionalized nanoparticles (NPs) are highly desirable owing to their potential applications in various fields including photonic materials,[64] electronic devices,[65] biosensors,[66] and template fabrication.[67] Figure 9 shows the SEM images of different patterns inscribed on the films. The patterns can be conveniently made which can span over $cm^2$ area. This can be used as a reproducible SERS substrate if SERS active nanoparticles can be incorporated in the patterns. RGO can act as a substrate to quench the fluorescence in resonance Raman spectroscopy, enhancing the utility of the patterned films fabricated.[68] Work in this direction is in progress. Luminescent patterns can also be fabricated through this methodology by incorporating NLf/Au@NLf in the composite (Supporting Information Figure S12). The inscribed pattern can be erased from the films and another pattern can be inscribed. Erasable and rewritable patterns may be useful in security coding and confidential data transfer.[69] Figure 10A and B show the film after imprinting the first pattern. The pattern was erased by simply wetting of the film using water. After drying the film, second pattern was inscribed. Figure 10C and D show the SEM images of this pattern. This pattern was also erased by wetting the film and next pattern was inscribed (Figure10 E and F). The film after erasure also was analyzed using SEM (Supporting Information S13). No trace of imprinted pattern was seen, pointing to the complete erasure of the pattern. The erasure and patterning can be done repeatedly. The Raman measurement clearly shows that the formed patterns are luminescent and the luminescence will not change even after imprinting and erasure events.

Creation of erasable patterns with properties such as luminescence, Raman activity, electrical conductivity, optical transparency, and other attributes may be useful in developing applications. No significant change in luminescence intensity was seen when exposed to a wide range of metal ions, change in pH (5−9), and temperature (10−50 °C). Such stable luminescent composites may be useful in security related applications such as bar-coding. The most used and the standard bar code normally employs a series of parallel bars, dark and light bars of different widths, for encoding a bit string. Bar-codes formatted as two-dimensional matrices are also in use. Fluorescent bar-codes are of recent origin and less commonly used. Unlike standard bar-code identifiers of adjacent black and white bands that are visible to the human eye under normal lighting conditions, the fluorescent nanomaterials may not be observable under normal light. Such bar-coding systems are particularly desirable as an invisible tag for valuable products or classified information.[69] Other advantage of using fluorescent bar-codes is that it does not require a plane background as in the case of standard bar-code and hence can be printed anywhere in the product without worrying the obstruction of printed matter on the product. Apart from using nanomaterials as fluorescent inks to inscribe bar-code patterns, other methods of patterning are also developed. In one such development, porous membranes have been used as templates for the preparation of encoded metal nanowires with a large number of distinguishable patterns.[70] The large-area films may be used to make such patterns in our composites film with appropriated modifications.

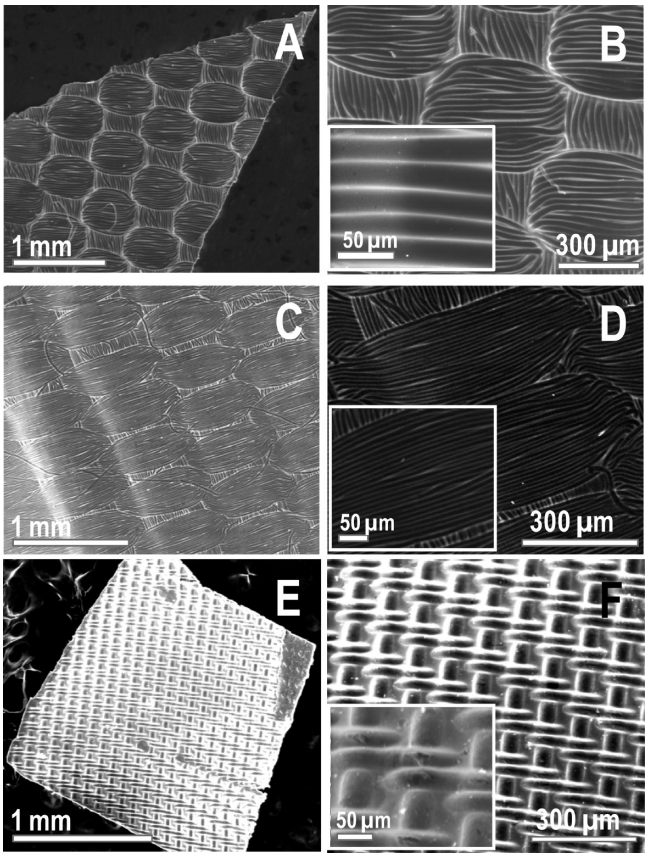


**Figure 10.** SEM images of the same part of the films showing the fabrication of erasable patterns. Left is large area image and the right is the corresponding enlarged image. In the left side images, only one edge of the free-standing composite film is shown. The area outside the film is the carbon tape used for fixing the film.

## CONCLUSIONS

A multifunctional GO/RGO based composite was fabricated. Different functionalities were added to GO/RGO by anchoring different materials such as native lactoferrin (NLf) or NLf protected Au cluster (Au@NLf) and/or chitosan (Ch). Electrostatic interaction at favorable pH resulted in the formation of the composites. Anchoring Au@NLf cluster resulted in the addition of luminescence functionality to RGO. A biocompatible polysaccharide, Ch was added to increase the dispersibility and enhance the properties. The composite was found to be an excellent antibacterial material. As-synthesized composites were molded into large area films ($cm^2$ area) through a simple solvent evaporation technique. The transmittance of the film can be modulated by controlling the concentration of RGO/GO added, opening up the possibility of applications in transparent conducting electrodes. Luminescent transparent RGO based films were also fabricated. The luminescence is stable against a variety of ions, pH, temperature, etc. enabling stable luminescent bar-coding applications. Erasable patterns were inscribed on the film. Luminescent patterns can be inscribed on the film and can be

erased by simply wetting the film. All of these diverse possibilities are important in developing applications.

## ■ ASSOCIATED CONTENT

**Supporting Information.** Detailed procedure for the preparation of GO, RGO, and sulfonation of RGO, Characterization of Au@NLf quantum clusters, IR spectra of GO, RGO, sulfonated RGO, TEM images of GO and RGO, Raman spectra of GO, RGO, $RGO_s$, UV/vis spectral changes of GO/RGO upon addition of Au@NLf, time-dependent TEM of RGO-Au@NLf upon e-beam irradiation, IR spectra of Ch containing composites, photograph showing the antibacterial activity of the composite, photoluminescence spectrum of the parent materials, XPS spectrum in Au 4f region from RGO-Au@NLf-Ch composite Raman characterization of luminescent patterns and SEM image of film after erasure. This material is available free of charge via the Internet at http://pubs.acs.org.

## ■ AUTHOR INFORMATION

**Corresponding Author**
*E-mail: pradeep@iitm.ac.in.

## ■ ACKNOWLEDGMENT

We thank the Nanoscience and Nanotechnology Initiative of DST, Government of India, for supporting our research program.

## ■ REFERENCES

(1) Novoselov, K. S.; Geim, A. K.; Morozov, S. V.; Jiang, D.; Zhang, Y.; Dubonos, S. V.; Grigorieva, I. V.; Firsov, A. A. *Science* **2004**, *306*, 666–669.
(2) Subrahmanyam, K. S.; Vivekchand, S. R. C.; Govindaraj, A.; Rao, C. N. R. *J. Mater. Chem.* **2008**, *18*, 1517–1523.
(3) Rao, C. N. R.; Sood, A. K.; Subrahmanyam, K. S.; Govindaraj, A. *Angew. Chem., Int. Ed.* **2009**, *48*, 7752–7777.
(4) Ghosh, A.; Subrahmanyam, K. S.; Krishna, K. S.; Datta, S.; Govindaraj, A.; Pati, S. K.; Rao, C. N. R. *J. Phys. Chem. C* **2008**, *112*, 15704–15707.
(5) Meyer, J. C.; Geim, A. K.; Katsnelson, M. I.; Novoselov, K. S.; Booth, T. J.; Roth, S. *Nature* **2007**, *446*, 60–63.
(6) Geim, A. K.; Novoselov, K. S. *Nat. Mater.* **2007**, *6*, 183–191.
(7) Lee, C.; Wei, X.; Kysar, J. W.; Hone, J. *Science* **2008**, *321*, 385–388.
(8) Zhang, Y.; Tan, Y.-W.; Stormer, H. L.; Kim, P. *Nature* **2005**, *438*, 201–204.
(9) Novoselov, K. S.; Geim, A. K.; Morozov, S. V.; Jiang, D.; Katsnelson, M. I.; Grigorieva, I. V.; Dubonos, S. V.; Firsov, A. A. *Nature* **2005**, *438*, 197–200.
(10) Balandin, A. A.; Ghosh, S.; Bao, W.; Calizo, I.; Teweldebrhan, D.; Miao, F.; Lau, C. N. *Nano Lett.* **2008**, *8*, 902–907.
(11) Han, M. Y.; Ouml; zyilmaz, B.; Zhang, Y.; Kim, P. *Phys. Rev. Lett.* **2007**, *98*, 206805.
(12) Li, X.; Cai, W.; An, J.; Kim, S.; Nah, J.; Yang, D.; Piner, R.; Velamakanni, A.; Jung, I.; Tutuc, E.; Banerjee, S. K.; Colombo, L.; Ruoff, R. S. *Science* **2009**, *324*, 1312–1314.
(13) Li, D.; Muller, M. B.; Gilje, S.; Kaner, R. B.; Wallace, G. G. *Nat. Nanotechnol.* **2008**, *3*, 101–105.
(14) Sreeprasad, T. S.; Samal, A. K.; Pradeep, T. *J. Phys. Chem. C* **2009**, *113*, 1727–1737.
(15) Hernandez, Y.; Nicolosi, V.; Lotya, M.; Blighe, F. M.; Sun, Z.; De, S.; McGovern, I. T.; Holland, B.; Byrne, M.; Gun'Ko, Y. K.; Boland, J. J.; Niraj, P.; Duesberg, G.; Krishnamurthy, S.; Goodhue, R.; Hutchison, J.; Scardaci, V.; Ferrari, A. C.; Coleman, J. N. *Nat. Nanotechnol.* **2008**, *3*, 563–568.
(16) Zhang, W.; Cui, J.; Tao, C.-a.; Wu, Y.; Li, Z.; Ma, L.; Wen, Y.; Li, G. *Angew. Chem., Int. Ed.* **2009**, *48*, 5864–5868.
(17) Lin, Y. M.; Dimitrakopoulos, C.; Jenkins, K. A.; Farmer, D. B.; Chiu, H. Y.; Grill, A.; Avouris, P. *Science* **2010**, *327*, 662.
(18) He, Q.; Sudibya, H. G.; Yin, Z.; Wu, S.; Li, H.; Boey, F.; Huang, W.; Chen, P.; Zhang, H. *ACS Nano* **2010**, *4*, 3201–3208.
(19) Yin, Z.; Wu, S.; Zhou, X.; Huang, X.; Zhang, Q.; Boey, F.; Zhang, H. *Small* **2010**, *6*, 307–312.
(20) Wang, X.; Zhi, L.; Mullen, K. *Nano Lett.* **2008**, *8*, 323–327.
(21) Schedin, F.; Geim, A. K.; Morozov, S. V.; Hill, E. W.; Blake, P.; Katsnelson, M. I.; Novoselov, K. S. *Nat. Mater.* **2007**, *6*, 652–655.
(22) Sreeprasad, T. S.; Maliyekkal, S. M.; Lisha, K. P.; Pradeep, T. *J. Hazard. Mater.* **2011**, *186*, 921–931.
(23) Chandra, V.; Park, J.; Chun, Y.; Lee, J. W.; Hwang, I.-C.; Kim, K. S. *ACS Nano* **2010**, *4*, 3979–3986.
(24) Hu, W.; Peng, C.; Luo, W.; Lv, M.; Li, X.; Li, D.; Huang, Q.; Fan, C. *ACS Nano* **2010**, *4*, 4317–4323.
(25) Liu, Z.; Robinson, J. T.; Sun, X.; Dai, H. *J. Am. Chem. Soc.* **2008**, *130*, 10876–10877.
(26) Agarwal, S.; Zhou, X.; Ye, F.; He, Q.; Chen, G. C. K.; Soo, J.; Boey, F.; Zhang, H.; Chen, P. *Langmuir* **2010**, *26*, 2244–2247.
(27) Chen, H.; Müller, M. B.; Gilmore, K. J.; Wallace, G. G.; Li, D. *Adv. Mater.* **2008**, *20*, 3557–3561.
(28) Habeeb Muhammed, M.; Ramesh, S.; Sinha, S.; Pal, S.; Pradeep, T. *Nano Res.* **2008**, *1*, 333–340.
(29) Rao, T. U. B.; Nataraju, B.; Pradeep, T. *J. Am. Chem. Soc.* **2010**, *132*, 16304–16307.
(30) Xavier, P. L.; Chaudhari, K.; Verma, P. K.; Pal, S. K.; Pradeep, T. *Nanoscale* **2010**, *2*, 2769–2776.
(31) Muhammed, M. H. A.; Verma, P. K.; Pal, S. K.; Retnakumari, A.; Koyakutty, M.; Nair, S.; Pradeep, T. *Chem.—Eur. J.* **2010**, *16*, 10103–10112.
(32) Qian, Z. M.; Li, H.; Sun, H.; Ho, K. *Pharmacol. Rev.* **2002**, *54*, 561–587.
(33) Kovtyukhova, N. I.; Ollivier, P. J.; Martin, B. R.; Mallouk, T. E.; Chizhik, S. A.; Buzaneva, E. V.; Gorchinskiy, A. D. *Chem. Mater.* **1999**, *11*, 771–778.
(34) Zhou, Y.; Bao, Q.; Tang, L. A. L.; Zhong, Y.; Loh, K. P. *Chem. Mater.* **2009**, *21*, 2950–2956.
(35) Si, Y.; Samulski, E. T. *Nano Lett.* **2008**, *8*, 1679–1682.
(36) Bonaccorso, F.; Sun, Z.; Hasan, T.; Ferrari, A. C. *Nat Photon* **2010**, *4*, 611–622.
(37) Chang, H.; Tang, L.; Wang, Y.; Jiang, J.; Li, J. *Anal. Chem.* **2010**, *82*, 2341–2346.
(38) Liu, M.; Zhao, H.; Quan, X.; Chen, S.; Fan, X. *Chem. Commun.* **2010**, *46*, 7909–7911.
(39) Surewicz, W. K.; Mantsch, H. H.; Chapman, D. *Biochemistry* **1993**, *32*, 389–394.
(40) Ramasamy, P.; Guha, S.; Shibu, E. S.; Sreeprasad, T. S.; Bag, S.; Banerjee, A.; Pradeep, T. *J. Mater. Chem.* **2009**, *19*, 8456–8462.
(41) Khor, E.; Lim, L. Y. *Biomaterials* **2003**, *24*, 2339–2349.
(42) Aimin, C.; Chunlin, H.; Juliang, B.; Tinyin, Z.; Zhichao, D. *Clin. Orthop. Relat. R* **1999**, *366*, 239–247.
(43) Chiou, S.-H.; Wu, W.-T.; Huang, Y.-Y.; Chung, T.-W. *J. Microencapsul.* **2001**, *18*, 613–625.
(44) Xu, H. H. K.; Simon, C. G. *Biomaterials* **2005**, *26*, 1337–1348.
(45) Yang, X.; Tu, Y.; Li, L.; Shang, S.; Tao, X.-m. *ACS Appl. Mater. Interfaces* **2010**, *2*, 1707–1713.
(46) Han, D.; Yan, L.; Chen, W.; Li, W. *Carbohyd. Polym.* **2011**, *83*, 653–658.
(47) Moulder, J. F.; Stickle, W. F.; Soble, P. E.; Bomben, K. D. *Handbook of X-ray Photoelectron Spectroscopy*; Perkin-Elmer Corporation: Eden Prairie, MN, 1992.
(48) Stankovich, S.; Dikin, D. A.; Piner, R. D.; Kohlhaas, K. A.; Kleinhammes, A.; Jia, Y.; Wu, Y.; Nguyen, S. T.; Ruoff, R. S. *Carbon* **2007**, *45*, 1558–1565.

(49) Sreeprasad, T. S.; Samal, A. K.; Pradeep, T. *Chem. Mater.* **2009**, *21*, 4527–4540.
(50) Shan, C.; Yang, H.; Han, D.; Zhang, Q.; Ivaska, A.; Niu, L. *Langmuir* **2009**, *25*, 12030–12033.
(51) Kang, S. Y.; Kim, K. *Langmuir* **1998**, *14*, 226–230.
(52) Battoccio, C.; Iucci, M. D.; Monti, S; Carravetta, V; Polzonetti., G *J. Phys.: Conf. Ser.* **2008**, *100*, 052079.
(53) Cen, L.; Neoh, K. G.; Kang, E. T. *J. Biomed. Mater. Res. A* **2004**, *71A*, 70–80.
(54) Rosemary, M. J.; MacLaren, I.; Pradeep, T. *Langmuir* **2006**, *22*, 10125–10129.
(55) Ramstedt, M.; Cheng, N.; Azzaroni, O.; Mossialos, D.; Mathieu, H. J. r.; Huck, W. T. S. *Langmuir* **2007**, *23*, 3314–3321.
(56) Nair, A. S.; Binoy, N. P.; Ramakrishna, S.; Kurup, T. R. R.; Chan, L. W.; Goh, C. H.; Islam, M. R.; Utschig, T.; Pradeep, T. *ACS Appl. Mater. Interfaces* **2009**, *1*, 24133–2419.
(57) Wei, C.; Lin, W. Y.; Zainal, Z.; Williams, N. E.; Zhu, K.; Kruzic, A. P.; Smith, R. L.; Rajeshwar, K. *Environ. Sci. Technol.* **1994**, *28*, 934–938.
(58) Schipper, M. L.; Nakayama-Ratchford, N.; Davis, C. R.; Kam, N. W. S.; Chu, P.; Liu, Z.; Sun, X.; Dai, H.; Gambhir, S. S. *Nat. Nanotechnol.* **2008**, *3*, 216–221.
(59) AshaRani, P. V.; Low Kah Mun, G.; Hande, M. P.; Valiyaveettil, S. *ACS Nano* **2008**, *3*, 279–290.
(60) Kim, K. S.; Zhao, Y.; Jang, H.; Lee, S. Y.; Kim, J. M.; Kim, K. S.; Ahn, J.-H.; Kim, P.; Choi, J.-Y.; Hong, B. H. *Nature* **2009**, *457*, 706–710.
(61) Becerril, H. c. A.; Mao, J.; Liu, Z.; Stoltenberg, R. M.; Bao, Z.; Chen, Y. *ACS Nano* **2008**, *2*, 463–470.
(62) Sionkowska, A.; Wisniewski, M.; Skopinska, J.; Kennedy, C. J.; Wess, T. J. *J. Photochem. Photobiol., A* **2004**, *162*, 545–554.
(63) Kong, B.-S.; Yoo, H.-W.; Jung, H.-T. *Langmuir* **2009**, *25*, 11008–11013.
(64) Chan, Y.-H.; Chen, J.; Wark, S. E.; Skiles, S. L.; Son, D. H.; Batteas, J. D. *ACS Nano* **2009**, *3*, 1735–1744.
(65) Keren, K.; Berman, R. S.; Buchstab, E.; Sivan, U.; Braun, E. *Science* **2003**, *302*, 1380–1382.
(66) Park, J.-U.; Lee, J. H.; Paik, U.; Lu, Y.; Rogers, J. A. *Nano Lett.* **2008**, *8*, 4210–4216.
(67) Kershner, R. J.; Bozano, L. D.; Micheel, C. M.; Hung, A. M.; Fornof, A. R.; Cha, J. N.; Rettner, C. T.; Bersani, M.; Frommer, J.; Rothemund, P. W. K.; Wallraff, G. M. *Nat. Nanotechnol.* **2009**, *4*, 557–561.
(68) Xie, L.; Ling, X.; Fang, Y.; Zhang, J.; Liu, Z. *J. Am. Chem. Soc.* **2009**, *131*, 9890–9891.
(69) Klajn, R.; Wesson, P. J.; Bishop, K. J. M.; Grzybowski, B. A. *Angew. Chem.* **2009**, *121*, 7169–7173.
(70) Li, X.; Wang, T.; Zhang, J.; Zhu, D.; Zhang, X.; Ning, Y.; Zhang, H.; Yang, B. *ACS Nano* **2010**, *4*, 4350–4360.